A Boundary Integral Method for 3D Nonuniform Dielectric Waveguide Problems via the Windowed Green Function

Emmanuel Garza, Constantine Sideris, and Oscar P. Bruno

***Abstract*—This paper proposes an efficient boundary-integral based "windowed Green function" methodology (WGF) for the numerical solution of three-dimensional general electromagnetic problems containing dielectric waveguides. The approach, which generalizes a recently-introduced two-dimensional version of the method, provides a highly effective solver for such problems. In particular, using an auxiliary integral representation, the proposed method is able to accurately model incident mode excitation. On the basis of a smooth window function, the integral operators along the infinite waveguide boundaries are smoothly truncated, resulting in errors that decay faster than any negative power of the window size.**

***Index Terms*—Integral equations, optical waveguides, numerical analysis, Chebyshev approximation**

I. Introduction

In view of their ability to efficiently guide electromagnetic energy, dielectric (open) waveguides play central roles in many engineered electromagnetic systems, including antenna feeds, coaxial cable transmission lines, optical fibers and nanophotonic devices, among many others [1]–[5]. As discussed in what follows, however, the computational simulation of electromagnetic waveguides in three-dimensions (3D) has posed a number of significant challenges—mostly concerning accuracy and computational cost. Seeking to tackle this difficulty, this paper introduces an efficient boundary integral equation (BIE) Green-function based methodology for this problem. This method incorporates, as a central enabling element, a novel "windowed Green function" strategy (WGF)—previously demonstrated in the context of layered media in two and three dimensions, and for waveguide structures in two dimensions [6]–[9]—to handle the truncation of BIE integration domains for fully-vectorial problems involving 3D dielectric waveguides with arbitrary shapes and configurations.

Most of the existing approaches for waveguide simulation rely on volumetric discretizations and approximation of the differential form of Maxwell's equations [10], incorporating an absorbing condition, such as a Perfectly Matched Layer (PML) [11], [12], to truncate the computational domain and, in particular, all of the semi-infinite waveguides present in the structure. The approach thus requires use of large 3D computational domains, and, consequently, large numbers of spatial unknowns. Further, evaluation of propagation over such large computational domains, which may amount to tens or even hundreds of wavelengths in relevant applications, can lead to significant dispersion errors by accumulation, over many wavelengths, of the errors inherent in the derivative approximations used in Finite Difference and Finite Element methods at each discretization point. The time-domain versions of these methods that are often employed additionally suffer from dispersion and accuracy loss in the time variable. As a result, these approaches may require extremely fine meshes and associated high computing costs to maintain accuracy.

On the basis of the electromagnetic Green's function, on the other hand, boundary integral methods (BIE) can lead to significantly reduced numbers of unknowns, since they only require discretization of the interfaces between different materials. Additionally, BIE methods are virtually free of numerical dispersion, in view of the Green's function's ability to analytically propagate oscillatory fields to arbitrary distances. And, although in their straightforward implementations they lead to computing costs that grow quadratically with the discretization sizes (at least if iterative solvers such as GMRES [13] are used), BIE methods can be accelerated by a variety of techniques [14]–[17]. Unfortunately, the application of BIE methods has almost exclusively been restricted to systems with bounded scatterers, in view of the lack of a suitable condition for termination of the infinite computational domain arising from infinite boundary interfaces.

Several effective approaches have recently emerged for the BIE waveguide-truncation problem, however. These include the WGF method [6]–[9], the closely related integral PML method [18], and a physically-motivated "Surface Conductive Absorber" approach (SCA) [19], [20]. Other methods based on use of adiabatic absorbers in conjunction with *volumetric* integral formulations, have also been demonstrated [21], [22]. The WGF method relies on a reformulation of the waveguide BIE equations, which results as the Green's function is smoothly windowed to a compact support via multiplication by a "slow-rise" window function in the integration variable. This procedure, which only requires multiplication of the Green's function by an adequate smooth window function, effectively screens out infinite boundary portions without introducing nonphysical reflection points on the boundary of the truncation domain, and it thus yields super-algebraic convergence—that is, asymptotically, faster convergence than any negative power of the window size. (A detailed and motivated description of the WGF method, including demonstrations of its accuracy and a strategy for selection of algorithmic parameters, can be found in [6].) The integral PML contribution [18] operates on the basis of the same principle as the WGF method: in the integral PML case the windowing effect is achieved by complexifying the spatial variables starting at a certain distance along the waveguide, which results in decaying exponentials in the Green's function and thus provide the desired reflection-screening effect. The SCA approach [19], finally, incorporating a surface conductivity on the material interfaces sufficiently far along the waveguides, demonstrates decay rates of the order of $1/x^p$ with the distance x along the waveguide, with e.g. $4 \leq p \leq 8$ for screening of waveguide modes and with $p = 1$ for screening of reactive fields; see [19, Figs. 9, 10].

The present contribution generalizes the 2D WGF method for waveguides [7] to the fully-vectorial 3D counterpart. It shows that the approach can handle both illuminating beams and point sources, as well as direct mode illumination. The paper is organized as follows. Section II describes the integral representation of the fields and the associated integral equations over the unbounded waveguide boundaries, making a distinction between two types of illuminating fields, namely, beams and point sources on one hand, and direct mode sourcing, on the other. Section III describes the ideas underlying the windowing of integral operators, and it presents our implementations for the two types of incidence considered in this paper. Finally, section IV presents a variety of numerical examples that demonstrate the effectiveness and flexibility of the WGF method for geometrically complex waveguide structures.

CS gratefully acknowledges support by the National Science Foundation (1849965, 2047433) and the Air Force Office of Scientific Research (FA9550-20-1-0087). CS and EG gratefully acknowledge support by the National Science Foundation under Grant 2030859 to the Computing Research Association for the CIFellows Project. OB gratefully acknowledges support from NSF under contracts DMS-1714169 and DMS-2109831, by AFOSR under contract FA9550-21-1-0373 and by the NSSEFF Vannevar Bush Fellowship under contract N00014-16-1-2808.

E. Garza and C. Sideris are with the Department of Electrical and Computer Engineering, University of Southern California, Los Angeles, CA 90089 USA.

O.P. Bruno is with the Department of Computing and Mathematical Sciences, California Institute of Technology, Pasadena, CA 91125 USA.

II. Boundary Integral Formulation for Three-Dimensional Dielectric Waveguides

Our approach is based on Müller's frequency-domain integral formulation [23], [24] at a given temporal frequency ω, which follows from use of Green's representation theorems [25]. (A time dependence of the type $\exp(-i\omega t)$ is assumed and suppressed throughout.) For clarity, in our description we consider a waveguide structure consisting of a single core (interior) region Ω_i (containing a material of permittivity ε_i, magnetic permeability μ_i and spatial wavenumber k_i), and a single cladding (exterior) region Ω_e (containing material of permittivity ε_e, magnetic permeability μ_e and spatial wavenumber k_e), as depicted in Fig. 1. The *unbounded* interface between Ω_i and Ω_e and the corresponding normal pointing from the former to the latter are denoted by Γ and $\boldsymbol{n}$, respectively. The wavenumber is related to the frequency and material properties by the relation $k = \omega\sqrt{\varepsilon\mu}$. The generalization of these methods to structures including an arbitrary number of waveguides and dielectric materials does not pose major difficulties.

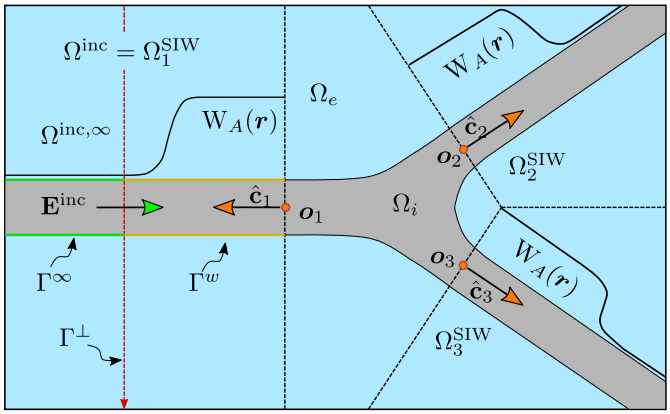

Fig. 1. Diagram of the windowing strategy and auxiliary domains used for bound mode excitation.

In this paper we consider two types of incident excitation, namely, *Type I excitation* by fields $(\mathbf{E}_i^{\text{inc}}, \mathbf{E}_e^{\text{inc}})$ (beams or point source incidence), for which the scattered fields $\mathbf{E}_i$ and $\mathbf{E}_e$ in the decomposition

$$\mathbf{E} = \mathbf{E}_i^{\text{inc}} + \mathbf{E}_i \quad \text{in } \Omega_i, \qquad \mathbf{E}_e^{\text{inc}} + \mathbf{E}_e \quad \text{in } \Omega_e \tag{1}$$

of the *total* electric field $\mathbf{E}$ are used as unknowns; and *Type II excitation* (Bound-mode incident field), for which the *total* electric fields

$$\mathbf{E} = \mathbf{E}_i \quad \text{in } \Omega_i, \qquad \mathbf{E}_e \quad \text{in } \Omega_e \tag{2}$$

themselves are used as unknowns.

Remark 2.1: For both type I and type II problems, the electromagnetic field can be expressed in terms of Green's function-based integral representations. The main difference in our treatment of these two cases is that for type II problems we use an integral representation of the *total* field (including the incident bound mode), whereas for type I problems we use an integral representation of the *scattered* field.

In order to introduce the aforementioned integral representations, we consider the following vector potentials acting on a surface tangential density $\boldsymbol{a}(\boldsymbol{r}')$:

$$\begin{aligned} \mathscr{A}_\ell[\boldsymbol{a}](\boldsymbol{r}) &\equiv \nabla \times \int_\Gamma G_\ell(\boldsymbol{r},\boldsymbol{r}')\boldsymbol{a}(\boldsymbol{r}')\mathrm{d}\sigma(\boldsymbol{r}'), \\ \mathscr{B}_\ell[\boldsymbol{a}](\boldsymbol{r}) &\equiv \nabla \times \nabla \times \int_\Gamma G_\ell(\boldsymbol{r},\boldsymbol{r}')\boldsymbol{a}(\boldsymbol{r}')\mathrm{d}\sigma(\boldsymbol{r}'). \end{aligned} \tag{3}$$

Here $G_\ell(\boldsymbol{r},\boldsymbol{r}') = \exp(ik_\ell|\boldsymbol{r}-\boldsymbol{r}'|)/(4\pi|\boldsymbol{r}-\boldsymbol{r}'|)$ denotes the free-space Helmholtz Green's function with wavenumber k_ℓ. Subscript values $\ell = i$ and $\ell = e$ indicate quantities corresponding to the interior and exterior domains, respectively.

The tangential values of the field (3) for $\boldsymbol{r} \in \Gamma$ are given by the boundary integral operators

$$\mathrm{S}_\ell[\boldsymbol{a}](\boldsymbol{r}) \equiv -\boldsymbol{n}(\boldsymbol{r}) \times \int_\Gamma G_\ell(\boldsymbol{r},\boldsymbol{r}')\boldsymbol{a}(\boldsymbol{r}')\mathrm{d}\sigma(\boldsymbol{r}'), \tag{4a}$$

$$\mathrm{R}_\ell[\boldsymbol{a}](\boldsymbol{r}) \equiv -\boldsymbol{n}(\boldsymbol{r}) \times \nabla \times \int_\Gamma G_\ell(\boldsymbol{r},\boldsymbol{r}')\boldsymbol{a}(\boldsymbol{r}')\mathrm{d}\sigma(\boldsymbol{r}'), \tag{4b}$$

$$\mathrm{T}_\ell[\boldsymbol{a}](\boldsymbol{r}) \equiv -\boldsymbol{n}(\boldsymbol{r}) \times \nabla \int_\Gamma G_\ell(\boldsymbol{r},\boldsymbol{r}')\,\mathrm{div}_\Gamma \boldsymbol{a}(\boldsymbol{r}')\mathrm{d}\sigma(\boldsymbol{r}'), \tag{4c}$$

which are defined for $\boldsymbol{r} \in \Gamma$. For conciseness, in what follows we also use the weakly-singular operators

$$\mathrm{R}_\alpha^\Delta \equiv \frac{2}{\alpha_e + \alpha_i}\left(\alpha_e\,\mathrm{R}_e - \alpha_i\,\mathrm{R}_i\right), \tag{5a}$$

$$\mathrm{K}_\alpha^\Delta \equiv \frac{2i}{\omega(\alpha_e+\alpha_i)}\left[(\mathrm{T}_e - \mathrm{T}_i) + (k_e^2\,\mathrm{S}_e - k_i^2\,\mathrm{S}_i)\right], \tag{5b}$$

where the subindex α stands either for the dielectric constant symbol, $\alpha = \varepsilon$, or the magnetic permeability symbol, $\alpha = \mu$. Finally, we call

$$\boldsymbol{m}_i \equiv -\boldsymbol{n} \times \mathbf{E}_i \;\text{ and }\; \boldsymbol{j}_i \equiv -\boldsymbol{n} \times \mathbf{H}_i \;\text{ on } \Gamma, \tag{6a}$$

$$\boldsymbol{m}_e \equiv +\boldsymbol{n} \times \mathbf{E}_e \;\text{ and }\; \boldsymbol{j}_e \equiv +\boldsymbol{n} \times \mathbf{H}_e \;\text{ on } \Gamma. \tag{6b}$$

the tangential magnetic and electric surface currents $\boldsymbol{m}_\ell$ and $\boldsymbol{j}_\ell$ on the interior ($\ell = i$) and exterior ($\ell = e$) sides of Γ.

Using these notations, the direct integral representations [25, theorem 5.5.1] (cf. the Stratton-Chu formulas [26, theorem 6.7]) for the exterior and interior fields are given by

$$\mathscr{A}_\ell[\boldsymbol{m}_\ell](\boldsymbol{r}) + \frac{i}{\omega\varepsilon_\ell}\mathscr{B}_\ell[\boldsymbol{j}_\ell](\boldsymbol{r}) = \begin{cases} \mathbf{E}_\ell(\boldsymbol{r}) & \boldsymbol{r} \in \Omega_\ell, \\ 0 & \boldsymbol{r} \notin \Omega_\ell, \end{cases} \tag{7a}$$

$$\mathscr{A}_\ell[\boldsymbol{j}_\ell](\boldsymbol{r}) - \frac{i}{\omega\mu_\ell}\mathscr{B}_\ell[\boldsymbol{m}_\ell](\boldsymbol{r}) = \begin{cases} \mathbf{H}_\ell(\boldsymbol{r}) & \boldsymbol{r} \in \Omega_\ell, \\ 0 & \boldsymbol{r} \notin \Omega_\ell, \end{cases} \tag{7b}$$

with $\ell = e$ and $\ell = i$, respectively. The Müller system of boundary integral equations results as a linear combination of the tangential limiting values of the fields in eq. (7) as $\boldsymbol{r} \to \Gamma$ from the exterior and interior domains [23], [24], [27]. The linear combination is selected in such a way that all the resulting integral operators are weakly-singular.

In the case of Type I excitation the continuity of the tangential components of the electromagnetic fields tells us that the unknown density currents satisfy the relations

$$\boldsymbol{m} \equiv \boldsymbol{m}_i = -\boldsymbol{m}_e + \boldsymbol{n} \times \left(\mathbf{E}_i^{\text{inc}} - \mathbf{E}_e^{\text{inc}}\right), \tag{8a}$$

$$\boldsymbol{j} \equiv \boldsymbol{j}_i = -\boldsymbol{j}_e + \boldsymbol{n} \times \left(\mathbf{H}_i^{\text{inc}} - \mathbf{H}_e^{\text{inc}}\right). \tag{8b}$$

The resulting Müller system for the Type I unknowns $\boldsymbol{m}$ and $\boldsymbol{j}$ reads

$$\begin{bmatrix} \mathrm{I} + \mathrm{R}_\varepsilon^\Delta & \mathrm{K}_\varepsilon^\Delta \\ -\mathrm{K}_\mu^\Delta & \mathrm{I} + \mathrm{R}_\mu^\Delta \end{bmatrix} \begin{bmatrix} \boldsymbol{m} \\ \boldsymbol{j} \end{bmatrix} = \begin{bmatrix} 2(\varepsilon_e+\varepsilon_i)^{-1}(\varepsilon_e\mathbf{E}_e^{\text{inc}} - \varepsilon_i\mathbf{E}_i^{\text{inc}}) \times \boldsymbol{n} \\ 2(\mu_e+\mu_i)^{-1}(\mu_e\mathbf{H}_e^{\text{inc}} - \mu_i\mathbf{H}_i^{\text{inc}}) \times \boldsymbol{n} \end{bmatrix}. \tag{9}$$

It is easy to check that this system involves only weakly-singular kernels; see e.g. [24], [9, chapter 5], [27].

For Type II excitation (that is, waveguide-mode incident fields) we utilize integral representations for the total fields, which incorporate integral expressions for the incident bound mode as well as the radiation conditions for waveguide problems—thus taking into account the directionality of incoming and outgoing modes [28].

Following [7], we assume that the waveguide structure includes one or more "semi-infinite waveguides" SIWGs). A SIWG is one half of an infinite waveguide (of arbitrary cross-section), as is obtained by cutting an ordinary infinite waveguide by a plane orthogonal to the optical axis. In addition to the SIWGs, the structure may contain arbitrary dielectric structures as long as all such structures are contained within a bounded region: away from such a bounded region, only the SIWGs break the homogeneity of space.

In view of these considerations, for the present incident-mode problems we define Ω^{inc} as the union of all SIWGs on which the incoming bound modes are given. Then, for both $\ell = i$ and $\ell = e$, the electric fields are characterized by the decomposition

$$\mathbf{E}_\ell = \begin{cases} \mathbf{E}_\ell^{\text{scat}} + \mathbf{E}_\ell^{\text{inc}} & \text{in } \Omega_\ell \cap \Omega^{\text{inc}}, \\ \mathbf{E}_\ell^{\text{scat}} & \text{in } \mathbb{R}^3 \setminus (\Omega_\ell \cap \Omega^{\text{inc}}), \end{cases} \tag{10}$$

with similar expressions for the magnetic fields $\mathbf{H}_\ell$. The integral representation in eq. (7) is still valid with the surface-current expressions in eq. (6), but, in the present incidence-mode case, $\mathbf{E}_\ell$ ($\ell = i, e$) represents the total field, not just the scattered component of the field. We can then re-express the unknown surface currents in terms of the scattered fields, by utilizing the known incident densities:

$$\boldsymbol{m} \equiv -\boldsymbol{n} \times \mathbf{E}_i^{\text{scat}} \;\text{ and }\; \boldsymbol{j} \equiv -\boldsymbol{n} \times \mathbf{H}_i^{\text{scat}} \;\text{ on } \Gamma, \tag{11a}$$

$$\boldsymbol{m}^{\text{inc}} \equiv -\boldsymbol{n} \times \mathbf{E}_i^{\text{inc}} \;\text{ and }\; \boldsymbol{j}^{\text{inc}} \equiv -\boldsymbol{n} \times \mathbf{H}_i^{\text{inc}} \;\text{ on } \Gamma. \tag{11b}$$

Just as in the case of type I sources, we must enforce the continuity of the tangential components of the fields, which implies that $\boldsymbol{m}_e = -(\boldsymbol{m} + \boldsymbol{m}^{\text{scat}})$ and $\boldsymbol{j}_e = -(\boldsymbol{j} + \boldsymbol{j}^{\text{scat}})$. Using the representation formula in eq. (7) and with the same derivation as for type I problems, we obtain the Müller system for type II incidence:

$$\begin{bmatrix} \mathrm{I} + \mathrm{R}_\varepsilon^\Delta & \mathrm{K}_\varepsilon^\Delta \\ -\mathrm{K}_\mu^\Delta & \mathrm{I} + \mathrm{R}_\mu^\Delta \end{bmatrix} \begin{bmatrix} \boldsymbol{m} \\ \boldsymbol{j} \end{bmatrix} = - \begin{bmatrix} \mathrm{I} + \mathrm{R}_\varepsilon^\Delta & \mathrm{K}_\varepsilon^\Delta \\ -\mathrm{K}_\mu^\Delta & \mathrm{I} + \mathrm{R}_\mu^\Delta \end{bmatrix} \begin{bmatrix} \boldsymbol{m}^{\text{inc}} \\ \boldsymbol{j}^{\text{inc}} \end{bmatrix}. \tag{12}$$

In order to produce a physical solution (e.g., to avoid the trivial solution $[\boldsymbol{m}, \boldsymbol{j}] = -[\boldsymbol{m}^{\text{inc}}, \boldsymbol{j}^{\text{inc}}]$), the scattered currents $\boldsymbol{m}$ and $\boldsymbol{j}$ must satisfy the *waveguide radiation conditions* [28, eq. (36)]. Briefly, these radiation conditions, which are a generalization of the Silver-Müller condition [23], state that the scattered solution must only consist of *outgoing* bound modes along the waveguide, and radiating fields away from the core region. The validity of both of these conditions in the WGF formulation results directly from its use of outgoing Green functions.

III. Windowing of Integral Operators

The numerical solution of eq. (9) over the unbounded waveguide boundary Γ requires careful consideration, in view of the slow decay rate—$\mathcal{O}(1/r)$—of the integrands in the associated integral operators. As discussed in this section, to do this, following [7], we: (1) localize the scattering problem to a bounded region encompassing the nonuniform parts of the waveguide structure, (2) use a *window* function to evaluate the slowly decaying, oscillatory integrals in the operators involving scattered currents, and (3) for type II problems (bound mode excitation) use the representation formula for the modes to evaluate the operators involving the incident currents from the bound mode.

The integrands in the integral operators eq. (4), which are defined over the *unbounded* boundary Γ, decay only as $\mathcal{O}(1/r)$ as $r \to \infty$, but they are also oscillatory, which makes their integrals finite. A direct truncation of the boundary Γ leads to extremely poor convergence—only $\mathcal{O}(1/\sqrt{A})$, where A denotes the SIWG-truncation length [7], [29]. However, *super-algebraic* convergence—$\mathcal{O}(A^{-p})$ for any positive integer p—can be regained on the basis of the same truncation size A, simply by multiplying the relevant integrands by a compactly supported, smooth "window" function. For strict super-algebraic convergence, the window function $w_A(d)$ must satisfy certain smoothness and "slow-rise" conditions [7, section III-B], namely, that the windowing function is smooth and that it decays from 1 to 0 over the region $d \in (\alpha A, A)$ for some $\alpha \in (0, 1)$. A suitable choice of window function that satisfies the conditions for super-algebraic convergence is given by the expression

$$w_A(d) \equiv \begin{cases} 1, & s(d) < 0, \\ \exp\left(-2\frac{\exp\left(-1/|s(d)|^2\right)}{|1-s(d)|^2}\right), & 0 \le s(d) \le 1\,, \\ 0, & s(d) > 1, \end{cases} \tag{13}$$

where $s(d) = (|d| - \alpha A)/(A - \alpha A)$; throughout this paper we utilize this window function with $\alpha = 0.5$ and $A = 10$. High-order convergence can also be achieved using other suitable window functions, such as the error function, that don't have strict compact support, but tend to zero exponentially fast at infinity.

As shown in [7], using a window function w_A can greatly improve the rate of convergence—so that oscillatory integrals along infinite domains can be accurately truncated by multiplying the integrand by w_A. On the other hand, although the convergence rate is "super-algebraic" (faster than any power of A), if the integrands are not sufficiently oscillatory, then large values of A may be necessary to achieve even modest accuracy. Hence, when the integrands might have vanishing oscillations—as it's the case of the right-hand-side of eq. (12)—a special treatment is required; see e.g. the third paragraph in [7, Sec. III(d)].

In the context of the three-dimensional waveguide problems considered in this paper, we can construct a suitable window function, denoted by $\mathrm{W}_A(\boldsymbol{r})$ for $\boldsymbol{r} \in \Gamma$, on the basis of the 1D window function eq. (13). Indeed, we first set $\mathrm{W}_A(\boldsymbol{r})$ to equal one when $\boldsymbol{r}$ is not in any of the SIWGs. Then, for $\boldsymbol{r}$ in a SIWG we set W_A equal to $w_A(d)$, where d denotes the distance from $\boldsymbol{r}$ to the plane perpendicular to the optical axis that determines the end of the SIWG. To define this mathematically, let M denote the total number of SIWGs, and let Ω_q^{SIWG} denote the domain that encompasses the q-th SIWG with its origin located at $\boldsymbol{o}_q$ and optical axis (pointing towards the infinite portion of the SIWG) along the $\hat{\boldsymbol{c}}_q$ direction. Then, we have

$$\mathrm{W}_A(\boldsymbol{r}) \equiv \begin{cases} w_A\left(\hat{\boldsymbol{c}}_q \cdot (\boldsymbol{r} - \boldsymbol{o}_q)\right), & \boldsymbol{r} \in \Gamma \cap \Omega_q^{\text{SIWG}}, \\ 1, & \text{otherwise.} \end{cases} \tag{14}$$

This definition of the window function for our waveguide problems leads in a natural way to a truncated domain for which the window is non-zero, i.e. $\Gamma^w = \Gamma \cap \{\boldsymbol{r} : \mathrm{W}_A(\boldsymbol{r}) > 0\}$. (For a different window function that does not have strict compact support, this definition of the truncated domain can be easily modified by taking the set for which $\mathrm{W}_A(\boldsymbol{r}) > \eta$, for some small tolerance $\eta > 0$.)

A. Type I Incidence: Direct Windowing

For the sake of simplicity, we assume incident fields for type I problems to have wavevectors with positive projections onto the optical axis $\hat{\boldsymbol{c}}_q$ of all the component SIWGs. This condition guarantees that the net oscillation of the integrands in the operators of eq. (9)—taking into account both the oscillation of the kernels and the solution currents—are bounded-away from zero, so that we can rely on windowing along the infinite boundary Γ to accurately truncate the simulation boundaries onto Γ^w. In the case that this condition is not met, such vanishing oscillations can be treated by means of an approach similar to the one used in [6] for layered media, or, simply, by re-scaling the infinite boundaries in terms of the net integrand wavenumber (net number of oscillations).

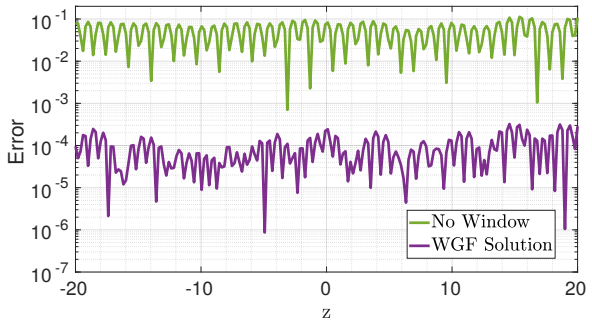

Fig. 2. Errors in the electric field $\mathbf{E}$ along the center of a straight waveguide with circular cross-section, obtained by comparison with the exact analytical solution. Purple line: errors resulting from the WGF (windowed-based) algorithm. Green line: errors obtained without use of windowing.

With the aforementioned assumption on the illuminating fields, we can directly window the integral operators on the left-hand side of eq. (9) to obtain

$$\begin{bmatrix} \mathrm{I}+\mathrm{R}_\varepsilon^\Delta \mathrm{W}_A & \mathrm{K}_\varepsilon^\Delta \mathrm{W}_A \\ -\mathrm{K}_\mu^\Delta \mathrm{W}_A & \mathrm{I}+\mathrm{R}_\mu^\Delta \mathrm{W}_A \end{bmatrix} \begin{bmatrix} \boldsymbol{m} \\ \boldsymbol{j} \end{bmatrix} = \begin{bmatrix} 2(\varepsilon_e+\varepsilon_i)^{-1}(\varepsilon_e \mathbf{E}_e^{\mathrm{inc}} - \varepsilon_i \mathbf{E}_i^{\mathrm{inc}}) \times \boldsymbol{n} \\ 2(\mu_e+\mu_i)^{-1}(\mu_e \mathbf{H}_e^{\mathrm{inc}} - \mu_i \mathbf{H}_i^{\mathrm{inc}}) \times \boldsymbol{n} \end{bmatrix}. \quad (15)$$

This system of integral equations over the *bounded* boundary Γ^w provides a super-algebraic approximation (w.r.t. the window size A) of the original, *unbounded* problem in the region of interest, i.e. where the nonuniform part of the structure is present. The system in eq. (15) can now be solved numerically using any bounded obstacle numerical method for integral equations.

Remark 3.1: In view of the definitions of the currents $\boldsymbol{j}$ and $\boldsymbol{m}$ in terms of the interior scattered fields in eq. (8), together with the waveguide radiation conditions discussed in section II, the currents behave asymptotically as the tangential components of a superposition of outgoing bound modes. The m-th mode contribution along the q-th SIWG contains a factor of $\exp\left(+ik_q^m|\hat{\boldsymbol{c}}_q \cdot \boldsymbol{r}'|\right)$ (where k_q^m denotes the propagation constant of the m-th mode). Since the integral kernels oscillate with a factor of $\exp\left(+ik|\boldsymbol{r}-\boldsymbol{r}'|\right)$, and since both k_q^m and k are positive, the product of the kernels and the currents result in non-vanishing oscillations as $\boldsymbol{r}|_\Gamma \to \infty$.

B. Type II Incidence: Accurate Evaluation of Incident Modes

This section proposes an integral equation methodology to accurately simulate the scattering of incident bound modes. To do this, windowing the integration domain in the same way as in section III-A, we split the integrals on the right-hand side of eq. (12) as the sum of two integrals—one over the bounded domain Γ^w and another over the unbounded domain Γ^∞ (noting that $\Gamma = \Gamma^w \cup \Gamma^\infty$). Let $\mathrm{R}_\alpha^{\Delta,w}$ and $\mathrm{R}_\alpha^{\Delta,\infty}$ denote the operators in eq. (5) but with the integration domains in eq. (4) substituted by Γ^w and Γ^∞, respectively. Using similar definitions for the K operator, we see that the right-hand side operators for the first equation in eq. (12) are given by

$$\mathrm{R}_\varepsilon^\Delta[\boldsymbol{m}^{\mathrm{inc}}](\boldsymbol{r}) + \mathrm{K}_\varepsilon^\Delta[\boldsymbol{j}^{\mathrm{inc}}](\boldsymbol{r}) = (\mathrm{R}_\varepsilon^{\Delta,w} + \mathrm{R}_\varepsilon^{\Delta,\infty})[\boldsymbol{m}^{\mathrm{inc}}](\boldsymbol{r}) + (\mathrm{K}_\varepsilon^{\Delta,w} + \mathrm{K}_\varepsilon^{\Delta,\infty})[\boldsymbol{j}^{\mathrm{inc}}](\boldsymbol{r}). \quad (16)$$

In this expression, the terms involving integrals over Γ^w can be easily computed, since the integration domain is bounded. On the other hand, the integrands decay slowly over the infinite surface Γ^∞ for target points $\boldsymbol{r}$ in the region of interest ($\boldsymbol{r} \in \Gamma^w$), and may have vanishing oscillations since the direction of the incoming mode is opposite to that of the oscillations from the integral kernels.

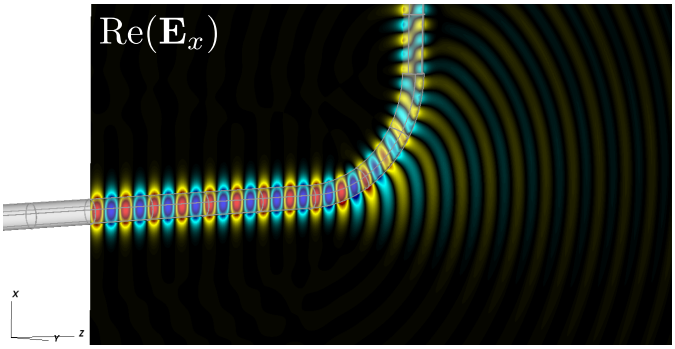

Fig. 3. Mode propagation along a 90° bend. The color scale for $|\mathbf{S}|$ and $\log|\mathbf{S}|$ goes from $A = 5\times10^{-6}$ to $B = 3\times10^{-1}$.

To evaluate the integrals over Γ^∞ with minimal error, we introduce an auxiliary representation for the incident modes. Let $\Gamma^\perp$ denote the orthogonal plane that cuts the incident SIWG at the end of Γ^w, and let $\Omega^{\mathrm{inc},\infty}$ denote the portion of Ω^{inc} that goes from $\Gamma^\perp$ towards the infinite side of the SIWG (see Fig. 1). Using the representation theorems for the electromagnetic fields [25] we obtain

$$(\mathscr{A}_\ell^\infty + \mathscr{A}_\ell^\perp)[\boldsymbol{m}_\ell^{\mathrm{inc}}](\boldsymbol{r}) + \frac{i}{\omega\varepsilon_\ell}(\mathscr{B}_\ell^\infty + \mathscr{B}_\ell^\perp)[\boldsymbol{j}_\ell^{\mathrm{inc}}](\boldsymbol{r}) = \begin{cases} \mathbf{E}_\ell^{\mathrm{inc}}(\boldsymbol{r}) & \boldsymbol{r} \in \Omega_\ell^{\mathrm{inc},\infty}, \\ 0 & \boldsymbol{r} \notin \Omega_\ell^{\mathrm{inc},\infty}. \end{cases} \quad (17)$$

For points $\boldsymbol{r} \in \Gamma^w$ (all of which are outside of $\Omega^{\mathrm{inc},\infty}$) we then have the relation

$$\mathscr{A}_\ell^\infty[\boldsymbol{m}_\ell^{\mathrm{inc}}](\boldsymbol{r}) + \frac{i}{\omega\varepsilon_\ell}\mathscr{B}_\ell^\infty[\boldsymbol{j}_\ell^{\mathrm{inc}}](\boldsymbol{r}) = -\mathscr{A}_\ell^\perp[\boldsymbol{m}_\ell^{\mathrm{inc}}](\boldsymbol{r}) - \frac{i}{\omega\varepsilon_\ell}\mathscr{B}_\ell^\perp[\boldsymbol{j}_\ell^{\mathrm{inc}}](\boldsymbol{r}) \quad (18)$$

which can be used to evaluate the right-hand side of eq. (12):

$$\mathrm{R}_\varepsilon^{\Delta,\infty}[\boldsymbol{m}^{\mathrm{inc}}](\boldsymbol{r}) + \mathrm{K}_\varepsilon^{\Delta,\infty}[\boldsymbol{j}^{\mathrm{inc}}](\boldsymbol{r}) = -\mathrm{R}_\varepsilon^{\Delta,\perp}[\boldsymbol{m}^{\mathrm{inc}}](\boldsymbol{r}) - \mathrm{K}_\varepsilon^{\Delta,\perp}[\boldsymbol{j}^{\mathrm{inc}}](\boldsymbol{r}). \quad (19)$$

Using a representation for the field $\mathbf{H}$ similar to the one used in eq. (17) for the field $\mathbf{E}$ we can obtain the right-hand side eq. (12) in terms of integrals along the bounded surface Γ^w and the unbounded boundary $\Gamma^\perp$. The resulting WGF version of eq. (12) reads

$$\begin{bmatrix} \mathrm{I}+\mathrm{R}_\varepsilon^\Delta \mathrm{W}_A & \mathrm{K}_\varepsilon^\Delta \mathrm{W}_A \\ -\mathrm{K}_\mu^\Delta \mathrm{W}_A & \mathrm{I}+\mathrm{R}_\mu^\Delta \mathrm{W}_A \end{bmatrix} \begin{bmatrix} \boldsymbol{m} \\ \boldsymbol{j} \end{bmatrix} = -\begin{bmatrix} \mathrm{I}+(\mathrm{R}_\varepsilon^{\Delta,w} - \mathrm{R}_\varepsilon^{\Delta,\perp}) & (\mathrm{K}_\varepsilon^{\Delta,w} - \mathrm{K}_\varepsilon^{\Delta,\perp}) \\ -(\mathrm{K}_\mu^{\Delta,w} - \mathrm{K}_\mu^{\Delta,\perp}) & \mathrm{I}+(\mathrm{R}_\mu^{\Delta,w} - \mathrm{R}_\mu^{\Delta,\perp}) \end{bmatrix} \begin{bmatrix} \boldsymbol{m}^{\mathrm{inc}} \\ \boldsymbol{j}^{\mathrm{inc}} \end{bmatrix}. \quad (20)$$

Remark 3.2: The operators on the right-hand side of eq. (20) involve integrals that can be accurately computed. The integrals over the bounded surface Γ^w can be treated as in the bounded obstacle case. On the other hand, the integrands over $\Gamma^\perp$, namely, the incident bound modes, decay *exponentially* as the distance to the interface tends to infinity—along $\Gamma^\perp$. This exponential decay allows us to evaluate integrals along $\Gamma^\perp$ by simple truncation, while incurring only exponentially small truncation errors.

IV. Numerical Examples

Any numerical discretization for boundary integral methods can be used to discretize the WGF integral equations: in particular, Galerkin, Nyström, or collocation method can be utilized. The illustrations

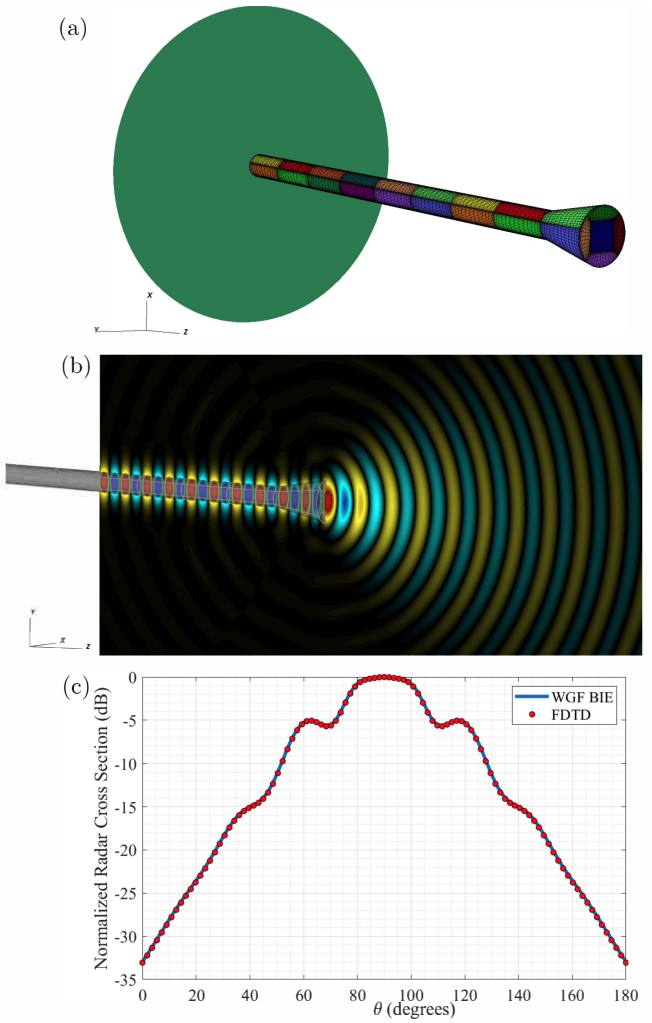

Fig. 4. Modeling of a waveguide-fed dielectric antenna. (a) Discretization of the structure, including the auxiliary circular surface $\Gamma^{\perp}$ used to evaluate the incident mode contribution. (b) Real part of $\mathbf{E}_x$. (c) Far-field RCS from $\theta = 0$ to π for $\phi = 0$, obtained by means of the the proposed approach and compared to the corresponding RCS produced via a commercial FDTD solver.

presented in this paper were produced by means of the discretization strategy presented in [27], [30], [31]. This approach relies on discretization of boundaries by a set of non-overlapping quadrilateral curvilinear patches that yields high-order convergence and can conveniently be applied to general CAD surface descriptions. The unknown current densities are discretized via Chebyshev polynomials on each surface patch. The far interactions are treated via Fejér's quadrature, and the near-singular and singular interactions are precomputed using a high-order quadrature rule for the weakly-singular integrals. Then, the system of integral equations is solved iteratively via GMRES.

This section presents several numerical examples that illustrate the accuracy and applicability of the proposed WGF approach. Our first example concerns a uniform circular waveguide, which allows us to provide comparisons with the analytical solution of a mode propagating unperturbed along the waveguide. In our second example we then consider a circular waveguide with a 90° bend. In a third example, we consider a dielectric antenna—e.g. an open waveguide with a termination—demonstrating the applicability of the method for this class of devices. The last example, finally, concerns a complex nanophotonic structure with multiple output waveguides. For all problems in this section we have assumed an exterior refractive index of 1.0 and a interior refractive index of 1.47 (SiO_2), with the exception of the last one for which the core is silicon ($n_{\text{Si}} = 3.47$) and the cladding is SiO_2 ($n_{\text{SiO}_2} = 1.44$).

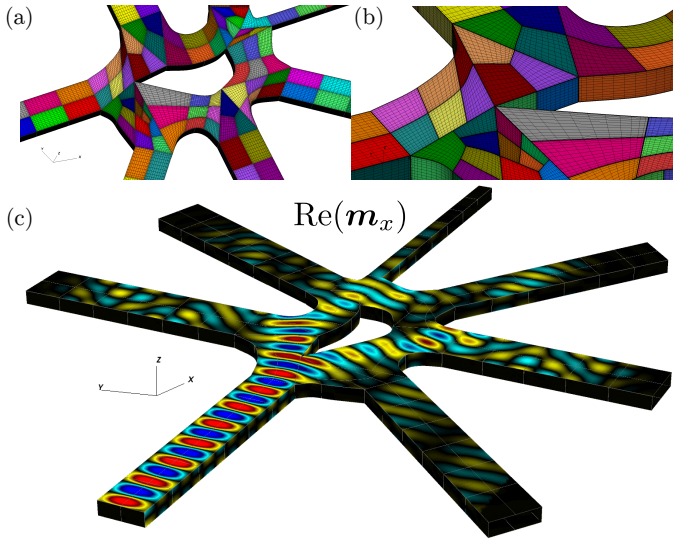

Fig. 5. Scattering by a complex silicon waveguide structure. Panels (a) and (b) display the patches used to discretize the geometry. The real part of the magnetic current $\boldsymbol{m}$ is shown in panel (c).

Fig. 2 presents, in purple color, the errors in the modal fields produced by the proposed window-based solver for a perfectly uniform waveguide with a circular cross section, along the line at the center of the waveguide. For this problem the modal fields may be expressed in terms of Bessel functions [5], [32], and the errors shown were obtained by comparison with this exact solution. Errors resulting from solutions without use of windowing but on the basis of the same spatial discretization are also presented in this figure, in green color; the beneficial effect of the windowing strategy can be appreciated easily. For this particular case, where a discretization of 18×18 (~ 9 points per mode's wavelength) is used, accuracies of order 10^{-4} are achieved by the WGF method, whereas errors of the order of 10^{-1} result from the un-windowed algorithm.

Fig. 3 presents simulation results for a circular waveguide with a 90° bend, illuminated by a bound mode. This figure presents the x-component of the electric field, and shows that the mode is mostly preserved across the curved region: the difference in character of the fields shown in the vertical and horizontal sections reflects the fact that the x-component of the field is the tangential component in the vertical section, but it is the normal component in the horizontal section.

Fig. 4 displays the fields resulting in a terminated open waveguide illuminated by a bound mode, i.e., a dielectric antenna. Fig. 4 (a) presents the discretization used as well as the auxiliary boundary $\Gamma^{\perp}$ utilized in this case to evaluate the right-hand side of eq. (20). Fig. 4 (b) presents the real part of $\mathbf{E}_x$, displaying, in particular, the near-field pattern and the energy radiation away from the waveguide termination region. Fig. 4 (c) plots the far-field radar cross section (RCS) produced by the proposed method as well as the one obtained via a well-known commercial FDTD solver. The proposed approach produced the solution with a far-field error of the order $1 \cdot 10^{-3}$ in a computing time of 21 seconds on 36 cores Xeon Gold 6154 and one Nvidia Titan V GPU. The FDTD solution, in turn, which does not support GPU acceleration, required 9.82 minutes on the same machine using all 36 cores. If preferred, the GPU acceleration in the present Green's-function implementation could be substituted by a Green's function acceleration method [14]–[17], for which we

expect similar overall computing times would result.

Our last example, which is presented in fig. 5, concerns a complex silicon structure, where all of the SIWGs have rectangular cross section. This example demonstrates the applicability of the WGF method to complex 3D nanophotonic structures. In order to handle the challenging geometrical features in this structure we utilized the CAD capabilities provided by Gmsh [33] to create the necessary patches shown in fig. 5 (a) and (b). The waveguide structure is illuminated by a Gaussian beam at the input port, and the real part of the magnetic current density is shown in fig. 5 (c).

V. Conclusions

We have presented a fully vectorial numerical method for the solution of complex 3D electromagnetic problems including waveguide structures on the basis of a windowed Green function boundary integral method. In this approach, the relevant integral operators—which are initially posed over the infinite boundaries of the waveguides—can be accurately evaluated, with super-algebraically small errors, by multiplying the integrands by a smooth window function and truncating the integration domain to the region where the window function does not vanish. In particular, we showed that incident mode excitation can be accurately incorporated by means of an auxiliary representation, which transform challenging integrals along the infinite boundary of the waveguide carrying the incident mode, onto integrals with exponentially decaying integrands. The ideas presented here are independent of the numerical discretization of the integral operators, and can indeed be used, in particular, in conjunction with any Nyström or Galerkin discretization, including the well-known method-of-moments approach.

References

[1] A. F. Koenderink, A. Alu, and A. Polman, "Nanophotonics: Shrinking light-based technology," *Science*, vol. 348, no. 6234, pp. 516–521, may 2015.

[2] R. M. Knox, "Dielectric waveguide microwave integrated circuits—an overview," *IEEE Trans. Microw. Theory Techn.*, vol. 24, no. 11, pp. 806–814, 1976.

[3] T. Itoh, "Application of gratings in a dielectric waveguide for leaky-wave antennas and band-reject filters," *IEEE Trans. Microw. Theory Techn.*, vol. 25, no. 12, pp. 1134–1138, 1977.

[4] C. R. Doerr and H. Kogelnik, "Dielectric waveguide theory," *J. Lightw. Technol.*, vol. 26, no. 9, pp. 1176–1187, 2008.

[5] A. W. Snyder and J. D. Love, *Optical Waveguide Theory*, 1st ed. New York: Chapman and Hall, 1983.

[6] O. P. Bruno, M. Lyon, C. Pérez-Arancibia, and C. Turc, "Windowed green function method for layered-media scattering," *SIAM Journal on Applied Mathematics*, vol. 76, no. 5, pp. 1871–1898, Jan. 2016.

[7] O. P. Bruno, E. Garza, and C. Pérez-Arancibia, "Windowed Green function method for nonuniform open-waveguide problems," *IEEE Trans. Antennas Propag.*, vol. 65, no. 9, pp. 4684–4692, 2017.

[8] C. Sideris, E. Garza, and O. P. Bruno, "Ultrafast simulation and optimization of nanophotonic devices with integral equation methods," *ACS Photonics*, vol. 6, no. 12, pp. 3233–3240, 2019.

[9] E. Garza, "Boundary integral equation methods for simulation and design of photonic devices," Ph.D. dissertation, California Institute of Technology, 2020.

[10] K. Bierwirth, N. Schulz, and F. Arndt, "Finite-difference analysis of rectangular dielectric waveguide structures," *IEEE Trans. Microw. Theory Techn.*, vol. 34, no. 11, pp. 1104–1114, 1986.

[11] J.-P. Berenger, "A perfectly matched layer for the absorption of electromagnetic waves," *J. Comput. Phys.*, vol. 114, no. 2, pp. 185–200, Oct. 1994.

[12] A. Taflove and S. C. Hagness, *Computational Electrodynamics: The Finite-Difference Time-Domain Method*, 3rd ed. Norwood: Artech House, Inc., 2005.

[13] Y. Saad and M. H. Schultz, "GMRES: A generalized minimal residual algorithm for solving nonsymmetric linear systems," *SIAM J. Sci. Stat. Comput.*, vol. 7, no. 3, pp. 856–869, 1986.

[14] L. Greengard and V. Rokhlin, "A fast algorithm for particle simulations," *J. Comput. Phys.*, vol. 73, no. 2, pp. 325–348, Dec. 1987.

[15] N. A. Gumerov and R. Duraiswami, *Fast Multipole Methods for the Helmholtz Equation in Three Dimensions*, 1st ed. Kidlington, Oxford: Elsevier Ltd., 2004.

[16] O. P. Bruno and L. A. Kunyansky, "A fast, high-order algorithm for the solution of surface scattering problems: Basic implementation, tests, and applications," *J. Comput. Phys.*, vol. 169, no. 1, pp. 80–110, May 2001.

[17] C. Bauinger and O. P. Bruno, "Interpolated factored green function method for accelerated solution of scattering problems," *Journal of Computational Physics*, vol. 430, p. 110095, 2021.

[18] W. Lu, Y. Y. Lu, and J. Qian, "Perfectly matched layer boundary integral equation method for wave scattering in a layered medium," *SIAM J. Appl. Math.*, vol. 78, no. 1, pp. 246–265, 2018.

[19] L. Zhang, J. H. Lee, A. Oskooi, A. Hochman, J. K. White, and S. G. Johnson, "A novel boundary element method using surface conductive absorbers for full-wave analysis of 3-D nanophotonics," *J. Lightw. Technol.*, vol. 29, no. 7, pp. 949–959, Apr. 2011.

[20] L. Zhang, "A boundary element method with surface conductive absorbers for 3-D analysis of nanophotonics," Ph.D. dissertation, Massachusetts Institute of Technology, 2010.

[21] A. Tambova, "The numerical modeling of nanophotonic structures by means of well-conditioned volume integral equation methods," Ph.D. dissertation, Skolkovo Institute of Science and Technology, 2019.

[22] A. Tambova, S. P. Groth, J. K. White, and A. G. Polimeridis, "Adiabatic absorbers in photonics simulations with the volume integral equation method," *J. Lightw. Technol.*, vol. 36, no. 17, pp. 3765–3777, Sep. 2018.

[23] C. Müller, *Foundations of the mathematical theory of electromagnetic waves*, 1st ed. Berlin, NY: Springer-Verlag, 1969.

[24] P. Ylä-Oijala and M. Taskinen, "Well-conditioned Müller formulation for electromagnetic scattering by dielectric objects," *IEEE Trans. Antennas Propag.*, vol. 53, no. 10, pp. 3316–3323, 2005.

[25] J.-C. Nédélec, *Acoustic and Electromagnetic Equations: Integral Representations for Harmonic Problems*, 1st ed. Springer, 2001.

[26] D. L. Colton, R. Kress, and R. Kress, *Inverse acoustic and electromagnetic scattering theory*, 3rd ed. Springer, 2013.

[27] J. Hu, E. Garza, and C. Sideris, "A Chebyshev-Based High-Order-Accurate Integral Equation Solver for Maxwell's Equations," *IEEE Trans. Antennas Propag.*, vol. 69, no. 9, pp. 5790–5800, Sep. 2021.

[28] A. I. Nosich, "Radiation conditions, limiting absorption principle, and general relations in open waveguide scattering," *Journal of electromagnetic waves and applications*, vol. 8, no. 3, pp. 329–353, Jan. 1994.

[29] J. A. Monro, "A super-algebraically convergent, windowing-based approach to the evaluation of scattering from periodic rough surfaces," Ph.D. dissertation, California Institute of Technology, 2007.

[30] O. P. Bruno and E. Garza, "A Chebyshev-based rectangular-polar integral solver for scattering by geometries described by non-overlapping patches," *J. Comput. Phys.*, vol. 421, p. 109740, Nov. 2020.

[31] E. Garza, J. Hu, and C. Sideris, "High-order Chebyshev-based Nyström Methods for Electromagnetics," in *2021 International Applied Computational Electromagnetics Society Symposium (ACES)*. IEEE, Sep. 2021, pp. 1–4.

[32] J. D. Jackson, *Classical Electrodynamics*, 3rd ed. Hoboken, New Jersey: John Wiley & Sons, Inc., 1998.

[33] C. Geuzaine and J.-F. Remacle, "Gmsh: A 3-D finite element mesh generator with built-in pre-and post-processing facilities," *International journal for numerical methods in engineering*, vol. 79, no. 11, pp. 1309–1331, 2009.